

Simultaneous position and state measurement of Rydberg atoms

C. S. E. van Ditzhuijzen¹, A. F. Koenderink², L. D. Noordam¹, and H. B. van Linden van den Heuvell¹

¹ Van der Waals-Zeeman Institute, University of Amsterdam, Valckenierstraat 65, 1018 XE Amsterdam, The Netherlands

² Center for Nanophotonics, FOM Institute AMOLF, Kruislaan 407, 1098 SJ Amsterdam, The Netherlands

Received: December 2, 2024/ Revised version: date

Abstract. We present a technique for state-selective position detection of cold Rydberg atoms. Ground state Rb atoms in a magneto-optical trap are excited to a Rydberg state and are subsequently ionized with a tailored electric field pulse. This pulse selectively ionizes only atoms in e.g. the 54d state and not in the 53d state. The released electrons are detected after a slow flight towards a micro channel plate. From the time of flight of the electrons the position of the atoms is deduced. The state selectivity is about 20:1 when comparing 54d with 53d and the one-dimensional position resolution ranges from 6 to 40 μm over a range of 300 μm . This state selectivity and position resolution are sufficient to allow for the observation of coherent quantum excitation transport.

PACS. 32.80.Pj, 34.60.+z, 32.80.Rm

1 Introduction

Rydberg atoms are well-known for their large dipole moments. Strong dipole-dipole interaction leads to interesting novel phenomena in particular for cold atoms. Examples are the triggering of spontaneous plasma formation [1,2] and the so called dipole blockade of optical excitation of a Rydberg atom in the vicinity of an already present Rydberg atom [3,4,5,6]. Another example is the formation of macrodimers from two Rydberg atoms [7,8].

When the distances between the interacting Rydberg atoms are fixed, which is achieved by using laser cooled atoms, the dipole-dipole interaction can be coherent [9,10]. For a pair of atoms with two successive principal quantum numbers, both in the highest (or lowest) energy Stark state, the interaction leads to an exchange of states between the atoms; in other words one state hops from one atom to the next [9]. The time required for hopping of a state back and forth is approximately given by:

$$t_{hop} = 9\pi \frac{d^3}{n^4} \quad (1)$$

with t_{hop} in atomic units, d the distance between the atoms in atomic units and n the principal quantum number. For $n=60$ and $d=20 \mu\text{m}$ the hopping time is 2.8 μs . These mesoscopic numbers make a quantum information system with position-resolved Rydberg atoms feasible. An interesting system [9] is for example the hopping of one excitation (e.g. $n=61$ or $|1\rangle$ in qubit notation) on a lattice of lower Rydberg states (e.g. $n=60$ or $|0\rangle$). Another example is the diffusion of the $|1\rangle$ state in a random gas of atoms in state $|0\rangle$, which might show features of Anderson localization [11].

In this paper we present experimental results that are a first step towards exploration of the coherent evolution of systems of Rydberg atoms. We show that the position-dependent readout of $|0\rangle$ and $|1\rangle$ states is indeed possible. The possibility to create and measure Rydberg atoms in a position and state resolved way is demonstrated here by exciting a narrow region in a cold cloud of rubidium atoms to the 54d state. The one-dimensional position sensitive detection is done with a time-of-flight technique. Time of flight is our choice in favor of a position-sensitive multi-channel plate detector because of simplicity and compatibility with existing equipment.

The time-of-flight approach makes it difficult to combine these measurements with other time-resolved techniques. State resolution is therefore based on the threshold character of field ionization, rather than timing as in conventional ramped state selective field ionization (SFI) [12]. The combination of techniques leads to conflicting optimizations. In the remainder of this paper these problems will be quantified and solved.

2 State and position determination

We first focus on the state determination by SFI [12]. The electric field E in which a Rydberg atom ionizes is roughly given by the classical ionization threshold, which is at an energy of $U = -2\sqrt{E}$, in atomic units, and corresponds to a field of $E = 1/16n^4$. Due to Stark shifts, however, the energy of the state changes with the electric field and the ionization field is different. In non-hydrogenic atoms many Stark states couple with each other, forming a level scheme with many avoided crossings. The best state selec-

tivity is achieved when the crossings are traversed either all adiabatically or all diabatically. In the latter case the field has to be ramped up faster than technically convenient, so we choose to ramp the field very slowly. In the adiabatic case the energy stays approximately the same and the ionization field will just be $1/16n^4$.

For the time-of-flight method we use the same electric field that ionizes the atoms. The electric potential at the starting position determines the final kinetic energy of the electron, because its starting velocity is negligible. The velocity of the electron can be determined by measuring the time it takes to cover a certain distance. To magnify the arrival time differences beyond the instrumental time resolution we use a long flight path and take care that the electrons are very slow during flight. The latter is achieved by letting the flight take place in a flight tube which provides a potential along the flight path that is almost the same as at the starting position. The arrival time of the electrons as a function of the initial position x is approximately

$$t(x) = L \sqrt{\frac{m_e}{2e(Ex + V_0)}} \quad (2)$$

with L the length of the flight tube e the charge and m_e the mass of the electron, E the electric field and V_0 the potential at $x=0$ minus the potential on the flight tube.

For the time-of-flight technique the time of ionization has to be well defined. This is in contradiction with the slow field ramp needed for the state selective field ionization. Therefore we use a more advanced scheme for the combination of the two techniques: a slow field ramp brings the field just below the ionization limit of the $|1\rangle$ state, followed by a fast pulse to go above the limit of the $|1\rangle$ state. In addition, this pulse has to stay below the ionization limit of the $|0\rangle$ state, in order to detect the atoms in state $|1\rangle$ exclusively.

3 Experimental Setup

To make sure the atoms don't move on the relevant timescale of the experiment we use a magneto-optical trap (MOT) of ^{85}Rb atoms as our cold atom source. A typical rubidium MOT has a temperature below $300 \mu\text{K}$ [13], which corresponds to an average velocity of $0.3 \mu\text{m}/\mu\text{s}$. The atoms are loaded from a dispenser into the MOT, created at the intersection of three orthogonal pairs of counterpropagating σ^+ - σ^- laser beams at the center of a magnetic quadrupole field. The background pressure is $3 \cdot 10^{-8}$ mbar. Charged particles from the dispenser are removed by deflection in an electric field of 50 V/cm , which is shielded from its environment. The laser frequency is tuned about 13 MHz below the $5S_{1/2} (F=3) \rightarrow 5P_{3/2} (F=4)$ resonance. A repumping laser beam tuned to the $5S_{1/2} (F=2) \rightarrow 5P_{1/2} (F=3)$ resonance is added at the MOT center. The cooling laser and the repumping laser are both Toptica DL100 diode lasers at resp. 780 nm and 795 nm and are locked to the rubidium resonance with Doppler-free FM spectroscopy. During all measurements the cooling laser is

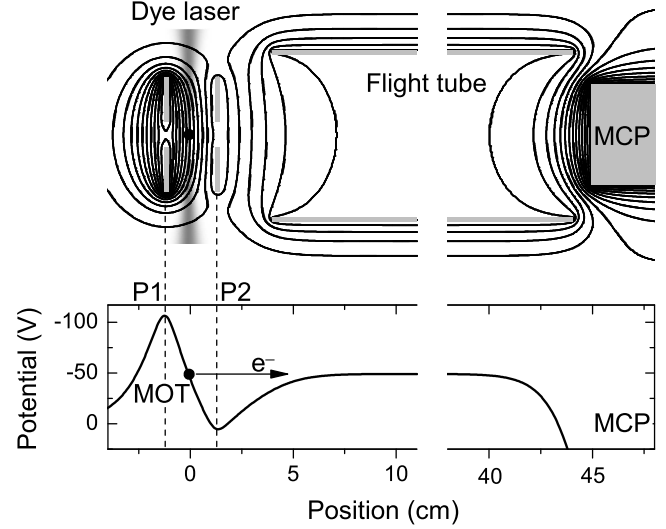


Fig. 1. Schematic representation of the components that provide the electric field together with equipotential lines, which are calculated numerically. The applied voltages are: -115 V on the first plate (P1), $+10 \text{ V}$ on the second plate (P2), -48 V on the flight tube and $+90 \text{ V}$ on the mesh in front of the MCP. Below is a graph of the electric potential on axis. Also depicted are the position of the MOT (black dot) and the dye laser beam.

blocked, so that all atoms are pumped to the $5S_{1/2} (F=3)$ ground state by the repumping laser.

To create atoms in a Rydberg state we excite cold atoms with an 8 ns , $2 \mu\text{J}$ laser pulse at 594 nm by a two-photon process from the $5s$ state to $53d$ or $54d$ (resp. $|0\rangle$ and $|1\rangle$). This light is provided by a Lambda Physik dye laser pumped with a Spectra Physics frequency-doubled, Q-switched Nd:YAG laser with a repetition rate of 10 Hz . The linewidth of the dye laser pulse is 0.15 cm^{-1} , which is well below the energy spacing between $53d$ and $54d$ (1.55 cm^{-1}). A small contamination of the nearest s-state, which lies 0.32 cm^{-1} higher, can not be excluded but is of no further relevance. The dye laser beam is focused in the MOT cloud by a lens placed on a micrometer translation stage. The beam waist is determined to be approximately $23(1) \mu\text{m}$ ($1/e$ diameter), measured with the knife-edge technique. The polarization of the light is parallel to the electric field that will be applied after the laser pulse.

The Rydberg atoms are field ionized by applying voltage pulses on two field plates P1 and P2 spaced by 2.5 cm (see Fig. 1). The circular stainless steel plates have a diameter of 5.5 cm and have a 1.4 cm hole in the middle for the transmission of one of the pairs of counterpropagating MOT laser beams. The released electrons go through the positively charged field plate P2 into a 40 cm long stainless steel tube, which is at negative potential and serves to slow down the electrons. After a 45 cm flight the electrons are detected on a Hamamatsu Micro Channel Plate (MCP). A copper mesh is placed in front of the MCP. The mesh is 95% open and set at $+90 \text{ Volt}$.

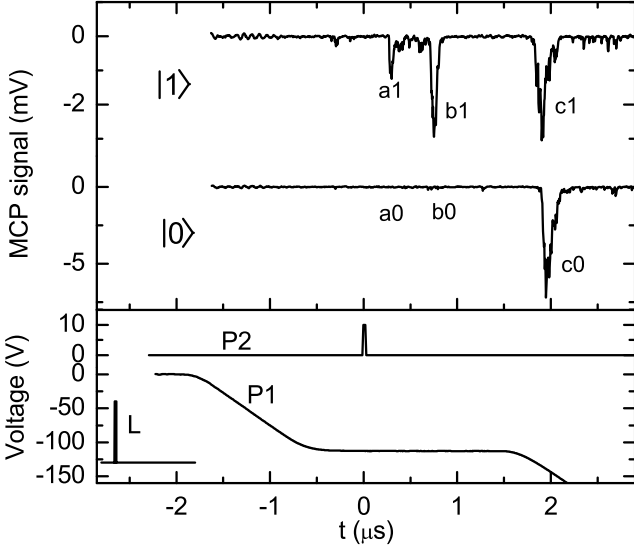


Fig. 2. In the lower panel the applied voltage pulses on the plates P1 and P2 are shown. The laser pulse is shown as L. In the upper panel the MCP signal for the $|0\rangle$ and $|1\rangle$ state (resp. 53d and 54d) are depicted. The first two peaks a and b are both resulting from the fast pulse on P2 at $t=0$. The peaks c originate from the atoms that are left over. The voltage on the flight tube is -48 V and the position of the dye laser beam is $280 \mu\text{m}$ on the scale of Fig. 3.

Additional coils outside the vacuum chamber compensate for background magnetic field. This is important for the electrons to fly straight towards the detector. The axis of the magnetic quadrupole field for the MOT is in the same direction as the electric field between the field plates.

For the simultaneous position and state detection we use the pulse scheme depicted in the lower half of Fig. 2. Shortly after the dye laser pulse we apply a slow voltage ramp on the field plate P1 which goes from 0 V to -115 V in $1.2 \mu\text{s}$. It then remains -115 V for $1.3 \mu\text{s}$, while a small, fast pulse is applied on the other plate P2. After that the voltage on the plate P1 is increased to -230 V in $1.2 \mu\text{s}$, to ionize all atoms that remained unionized. With the fast pulse we aim to ionize the upper state atoms exclusively at a well defined time. The slow ramp is provided by an Agilent 33240A amplified by a home-built amplifier system. The fast pulse is 10 V, with a duration of 30 ns and a rise time of 10 ns and is provided by an HP 8114A.

For the calibration of the conversion from time-of-flight to position we shift the Rydberg-production volume along the flight path by moving the lens that focuses the dye laser beam in the MOT cloud and record the signal of the MCP for every lens position. The voltage on the flight tube is carefully tuned, such that the electrons created at the edge of the MOT nearest to the plate P2 are still clearly detected on the MCP. This usually means that they have a flight time of $1 \mu\text{s}$, or equivalently, an energy of 0.5 eV. At lower velocities the signal density drops.

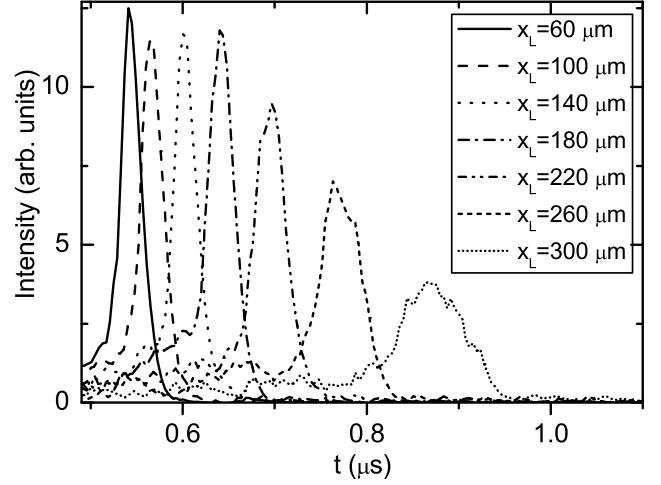


Fig. 3. Measured time-of-flight spectra for different laser focus positions x_L . The peaks correspond, apart from a minus, to the peak b1 as defined in Fig. 2. The time $t=0$ is when the 30 ns pulse is applied to plate P2.

4 Results

In the upper panel of Fig. 2 the MCP signal during the voltage pulses is depicted for two different dye laser wavelengths. The upper trace is the signal for $\lambda=594.166 \text{ nm}$, which excites to the 54d state or the $|1\rangle$ state and the trace below this is the signal for $\lambda=594.193 \text{ nm}$, leading to excitation of the 53d state or the $|0\rangle$ state.

The first two peaks, labelled a and b, both result from the fast pulse on plate P2. For the time-of-flight measurements we will focus on peak b, because this peak is most sensitive to the position of the Rydberg-production volume. Peak b1 consists of 30% of the total signal of state $|1\rangle$. When the atoms are prepared in state $|0\rangle$, the same measurement should ideally give no signal (b0). From our measurements we find an upper bound that is 1% or 2% of the total signal. The ratio of the genuine and spurious $|1\rangle$ signal is therefore about 20. In future experiments we will attempt to improve this ratio further. The spurious signal could result from atoms that are actually excited to the $|1\rangle$ state, due to the finite laser linewidth, or from atoms in the $|0\rangle$ state that ionize in a smaller field. The peaks c0 and c1 originate from atoms that were not ionized by the short pulse and are ionized by the subsequent ramp. This slow ramp lacks the possibility of position resolution, but is useful for estimating the ionization efficiency during the earlier pulses. The limited ionization of the upper state atoms by the fast pulse might be due to the limited pulse height and duration of this pulse.

Fig. 3 shows time-of-flight spectra for the state $|1\rangle$. The peaks correspond to the peak b1 as defined in Fig. 2 for several positions of the dye laser focus. It can be seen that for faster electrons the peaks are narrower, but also start to overlap more. The peaks in the time-of-flight spectrum appeared to be narrowest when the duration of the fast pulse applied on plate P2 was 30 ns.

We transformed the time-of-flight spectra to the position domain using Eq. 2 with $L=40 \text{ cm}$. As the potential is

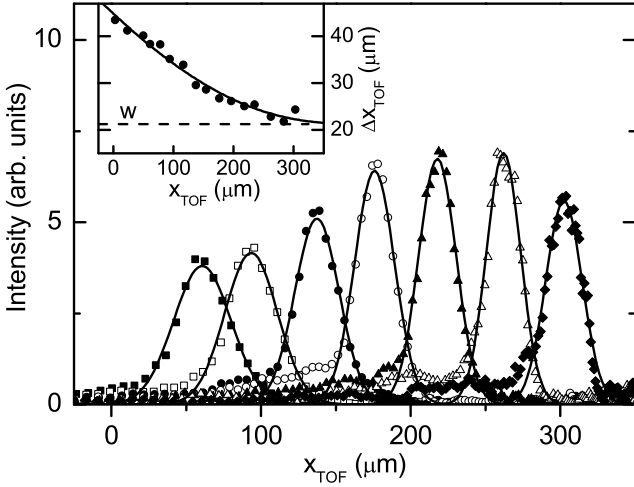


Fig. 4. The peaks of Fig. 3 are transformed to the position domain using Eq. 2. Solid lines show gaussian fits. In the inset the $1/e$ -widths of these gaussians Δx_{TOF} are plotted against the center position x_{TOF} . The solid line is a fit to the data with Eq. 3. The dashed line w shows the fitted width of the Rydberg-production volume ($21 \mu\text{m}$).

significantly more complicated (see Fig. 1) than assumed for the simple model of Eq. 2, we use an effective field E and V_0 as fit parameters. Also we add a short offset time of 13 ns, based on numerical calculations, for the parts of the flight that are outside the flight tube. Our fit is based on more traces than depicted in Fig. 3, since the measurements were taken for lens positions $20 \mu\text{m}$ apart. The peaks in the position domain can be excellently fitted with gaussian profiles, as shown in Fig. 4. Optimal agreement of the center positions of the fitted gaussians with the known 20 micron between lens positions is obtained for $E=50.2 \text{ V/cm}$ and $V_0=-2.2 \text{ V}$.

It can be seen that in the position domain the peaks get narrower for larger x (i.e. "downhill" on the potential in Fig. 1), while the corresponding peaks in the time domain (i.e. later times) get wider. For large x the broadening due to the finite width of the Rydberg-production volume w (due to a finite laser beam waist) is dominant. For small x the time broadening effect τ is dominant. This time width τ and not the Rydberg-production volume w is the limit for the spatial resolution of our time-of-flight system. Therefore we decouple τ from the widths Δx_{TOF} of the gaussians by fitting the two broadening effects to the following expression

$$\Delta x_{TOF} = \sqrt{w^2 + \left(\frac{dx(t)}{dt}\right)^2 \tau^2} \quad (3)$$

with $x(t)$ the inverse function of Eq. 2. In the inset of Fig. 4 Δx_{TOF} is plotted against the center position x_{TOF} together with the fitted dependence. The fitted parameters are $\tau=20(1) \text{ ns}$ and $w=21(1) \mu\text{m}$, which is comparable to $1/\sqrt{2}$ times the measured laser waist (the $1/\sqrt{2}$ factor originates from the two-photon character excitation).

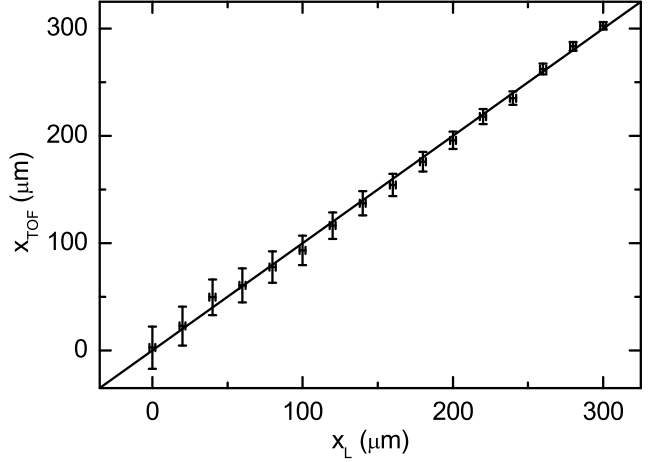


Fig. 5. The center positions of the fitted gaussians of Fig. 4 x_{TOF} plotted against the read-off position x_L . The solid line is $x_{TOF} = x_L$. The small horizontal error bar is an estimate of the read-off error ($2 \mu\text{m}$). The vertical error bars are obtained by transforming the fitted time width τ to position and give the spatial resolution of our system.

In Fig. 5 we plot the center positions of the gaussians x_{TOF} against the read-off position of the lens that focuses the dye laser beam into the MOT cloud (x_L), together with the line $x_{TOF} = x_L$. The data points show an excellent agreement with the straight line, which shows that the simple model Eq. 2 is well suited to the convert flight times into position. The small horizontal error bar is an estimate of the read-off error ($2 \mu\text{m}$). The vertical error bars provide the spatial resolution of our system and are obtained by transforming the time width τ to position. The spatial resolution ranges from 6 to $40 \mu\text{m}$ over a distance of $300 \mu\text{m}$ ($1/e$ diameter), and it is better than $20 \mu\text{m}$ over a range of $150 \mu\text{m}$.

5 Conclusions

We have demonstrated a technique for state-selective position detection of cold Rydberg atoms. The state selectivity is about 20:1 when comparing 54d with 53d and might be improved by using a narrower spectral linewidth of the Rydberg-exciting laser or by optimizing the electric field pulse sequence. The position resolution ranges from 6 to $40 \mu\text{m}$ over a distance of $300 \mu\text{m}$. These n-state and position resolution are sufficient to allow for the observation of long range hopping transport by coherent dipole-dipole interactions in cold Rydberg systems [9].

We thank F. Robicheaux for fruitful discussions and R. Kemper, A. de Snaijer and A. Gürtler for help in building the experimental setup. We thank the FOM Institute AMOLF for borrowing equipment. This work is part of the research program of the "Stichting voor Fundamenteel Onderzoek der Materie" (FOM), which is financially supported by the "Nederlandse Organisatie voor Wetenschappelijk Onderzoek" (NWO).

References

1. M. P. Robinson, B. L. Tolra, M. W. Noel, T. F. Gallagher and P. Pillet, *Phys. Rev. Lett.* **85**, 4466 (2000)
2. W. Li, P. J. Tanner, and T. F. Gallagher, *Phys. Rev. Lett* **94**, 173001 (2005)
3. D. Jaksch, J. I. Cirac, P. Zoller, S. L. Rolston, R. Côté and M. D. Lukin, *Phys. Rev. Lett* **85**, 2208 (2000)
4. M. D. Lukin, M. Fleischhauer, R. Côté, L. M. Duan, D. Jaksch, J. I. Cirac and P. Zoller, *Phys. Rev. Lett* **87**, 037901 (2001)
5. D. Tong, S. M. Farooqi, S. Krishan, Y. P. Zhang, R. Côté, E. E. Eyler and P. L. Gould, *Phys. Rev. Lett* **93**, 063001 (2004)
6. K. Singer, M. Reetz-Lamour, T. Amthor, L. G. Marcassa and M. Weidemüller, *Phys. Rev. Lett* **93**, 163001 (2004)
7. C. Boisseau, I. Simbotin and R. Côté, *Phys. Rev. Lett* **88**, 133004 (2002)
8. S. M. Farooqi, D. Tong, S. Krishnan, J. Stanojevic, Y. P. Zhang, J. R. Ensher, A. S. Estrin, C. Boisseau, R. Côté, E. E. Eyler and P. L. Gould, *Phys. Rev. Lett* **91**, 183002 (2003)
9. F. Robicheaux, J. V. Hernández, T. Topçu and L. D. Noordam, *Phys. Rev. A* **70**, 042703 (2004)
10. M. Mudrich, N. Zahzam, T. Vogt, D. Comparat and P. Pillet, *Phys. Rev. Lett* **95**, 233002 (2005)
11. P. W. Anderson, *Phys. Rev.* **109**, 1492 (1958)
12. T. F. Gallagher, *Rydberg Atoms* (Cambridge University Press, Cambridge, 1994)
13. C. D. Wallace, T. P. Dinneen, K. Y. N. Tan, A. Kumarakrishnan, P. L. Gould and J. Javanainen, *J. Opt. Soc. Am. B* **11**, 703 (1994)